*J. Fluid Mech.* (1979), *vol.* 91, *part* 1, *pp.* 155–165
*Printed in Great Britain*



# Three-dimensional convection in a cubic box of fluid-saturated porous material

By JOE M. STRAUS AND GERALD SCHUBERT†

Space Sciences Laboratory, The Ivan A. Getting Laboratories,
The Aerospace Corporation, Los Angeles, California 90009

(Received 25 May 1978 and in revised form 22 August 1978)

Calculations of finite amplitude convection in cubic boxes containing fluid-saturated porous material are reported for Rayleigh numbers $R$ as large as 150. Steady two- or three-dimensional convection can always be forced by appropriate choice of initial conditions. Randomly chosen initial conditions will result in either two- or three-dimensional convection. Although there is a non-uniqueness associated with initial conditions which makes possible either two- or three-dimensional convection, the non-uniqueness is limited in the sense that only one two-dimensional or one three-dimensional solution appears to be realizable. Two-dimensional flows have larger Nusselt numbers than three-dimensional flows for $R \lesssim 97$; the opposite is true for $R \gtrsim 97$.

## 1. Introduction

At present, we know relatively little about the nature of three-dimensional, finite amplitude thermal convection. Because of its intrinsic importance and its relevance to the general phenomenon, we have chosen to study such convection in cubic boxes of fluid-saturated porous material heated from below. According to linear theory, 'strictly' three-dimensional convection in a cubic box is possible only for $R > 4{\cdot}5\pi^2$ (Beck 1972). (For $R$ as small as $4\pi^2$, there can exist a trivial form of three-dimensional convection, consisting of the superposition of orthogonal two-dimensional rolls. For $R > 4{\cdot}5\pi^2$, our calculations never produced this form of convection.) We consider Rayleigh numbers $R$ which lie between the critical value of $4{\cdot}5\pi^2$ and 150. For these values of $R$, we have shown that there is always a stable form of steady two-dimensional convection (Straus & Schubert 1978). Thus, if three-dimensional convection were to exist at all at these Rayleigh numbers, there would have to be a non-uniqueness in the form of the convection pattern associated with initial conditions. That this is indeed the case is indicated by previous numerical studies. Holst & Aziz (1972) calculated both steady two-dimensional and steady three-dimensional flows in cubic boxes at $R = 60$ and $R = 120$; Horne (1978) also found both two- and three-dimensional steady convection in cubic boxes at $R = 75$ and 100.

Since stable, steady two-dimensional convection is always realizable, we have asked two questions concerning the existence of steady three-dimensional convection. Can steady three-dimensional convection always be realized by appropriate choice of

† Permanent address: Department of Earth and Space Sciences, University of California, Los Angeles, California 90024.

0022-1120/79/4169-5820 $02.00 

initial conditions? For a random choice of initial conditions will convection prefer to be two- or three-dimensional? Our results indicate that it is always possible to force either steady two-dimensional or steady three-dimensional convection by proper choice of initial conditions. We have also found that random initial conditions lead to either steady two-dimensional or steady three-dimensional convection.

Because two- and three-dimensional convection are always achievable states, it is important to compare the heat transported by each of them. Holst & Aziz (1972) reported that the two-dimensional Nusselt number was larger than the three-dimensional one at $R = 60$, but the reverse was true at $R = 120$. Horne (1978) also determined that the two-dimensional Nusselt number was larger than the three-dimensional one at $R = 75$, with the reverse true at $R = 100$. Our computations, which give $Nu$ accurate to 1 % up to $R = 150$, show that the heat transport by three-dimensional convection exceeds that by two-dimensional convection for $R \gtrsim 97$, while for $R \lesssim 97$ two-dimensional convection transports more heat. Zebib & Kassoy (1978) have used a two-term expansion of the temperature and velocity fields to demonstrate that the two-dimensional value of $Nu$ exceeds that for three-dimensional motion consisting of a superposition of orthogonal rolls when $R$ is slightly supercritical. It has been proposed by Malkus (1954) and Platzman (1965) that a flow will evolve to a steady configuration that maximizes the heat transport. There has been no rigorous demonstration of the validity of this proposal, and our results do not support it since we find that the system often chooses the state with the smaller Nusselt number when it is allowed to evolve from random initial conditions.

In the sections to follow we first develop the equations required to describe time-dependent three-dimensional convection in a box of fluid-saturated porous material using the Galerkin technique, and we then discuss the numerical solutions of these equations for cubic boxes and Rayleigh numbers as large as 150. In particular, we show details of the flow and temperature patterns for steady three-dimensional convection at $R = 80$ and 150, we compare $Nu$ *vs.* $R$ curves for two- and three-dimensional convection, and we discuss the dependence of the solutions on the choice of initial conditions.

## 2. Mathematical formulation

Consider a rectangular box of fluid-saturated permeable material heated from below. The bottom of the box is $z = 0$ and the top is $z = d$. The sides of the box are $x = 0$, $x = l$, $y = 0$ and $y = b$. We develop the equations for a box with arbitrary dimensions although we shall present numerical results only for cubic boxes. The top and bottom of the box are isothermal impermeable surfaces. The sides of the box are insulating impermeable boundaries. The temperatures $T$ of the top and bottom surfaces are $T_0$ and $T_0 + \Delta T$, respectively.

The equations governing convection in the box are

$$\nabla . \mathbf{u} = 0, \tag{1}$$

$$\nabla p + \rho\alpha(T - T_0 - \Delta T + \Delta T z/d)\,\mathbf{g} + (\mu/K)\,\mathbf{u} = 0, \tag{2}$$

$$\chi\,\partial T/\partial t + \rho c\mathbf{u} . \nabla T = k\nabla^2 T, \tag{3}$$

where the Darcy velocity $\mathbf{u}$ is the volumetric flow rate of fluid per unit area of the porous medium, $p$ is the pressure in excess of the hydrostatic value, $\rho$ is the fluid density, $\alpha$ is the thermal expansivity of the fluid, $\mathbf{g}$ is the acceleration due to gravity, $\mu$ is the viscosity of the fluid, $K$ is the permeability of the porous medium, $\chi$ is the average heat capacity per unit volume of the fluid and solid matrix, $c$ is the specific heat of the fluid, and $k$ is the average thermal conductivity of the fluid and solid matrix. The quantity $T_0+\Delta T-\Delta T\,z/d$ in the buoyancy term of (2) is, of course, just the conduction temperature profile. We have made the Boussinesq approximation and adopted Darcy's law in writing these equations. The boundary conditions are

$$T = T_0+\Delta T, \quad w = 0 \quad \text{on} \quad z = 0, \tag{4}$$

$$T = T_0, \quad w = 0 \quad \text{on} \quad z = d, \tag{5}$$

$$\partial T/\partial x = 0, \quad u = 0 \quad \text{on} \quad x = 0, l, \tag{6}$$

$$\partial T/\partial y = 0, \quad v = 0 \quad \text{on} \quad y = 0, b, \tag{7}$$

where $u$, $v$ and $w$ are the $x$, $y$ and $z$ components of the Darcy velocity.

We introduce the dimensionless quantities

$$\xi = \frac{x}{d}, \quad \eta = \frac{y}{d}, \quad \zeta = \frac{z}{d}, \quad \bar{\nabla} = d\nabla, \quad \tau = \frac{kt}{\chi d^2}, \tag{8}$$

$$\bar{u} = \frac{\rho c d}{k}u, \quad \bar{v} = \frac{\rho c d}{k}v, \quad \bar{w} = \frac{\rho c d}{k}w, \quad \bar{\mathbf{u}} = \frac{\rho c d}{k}\mathbf{u}, \tag{9}$$

$$\theta = \frac{T-T_0-\Delta T+\Delta T z/d}{\Delta T}, \qquad \pi = \frac{K\rho c}{\mu k}p, \tag{10}$$

in terms of which the equations and boundary conditions are

$$\bar{\nabla}.\bar{\mathbf{u}} = 0, \tag{11}$$

$$\bar{\nabla}\pi + \bar{\mathbf{u}} - R\theta\hat{\boldsymbol{\zeta}} = 0, \tag{12}$$

$$\partial\theta/\partial\tau + \bar{\mathbf{u}}.\bar{\nabla}\theta = \bar{w}+\bar{\nabla}^2\theta, \tag{13}$$

$$\theta = \bar{w} = 0 \quad \text{on} \quad \zeta = 0, 1, \tag{14}$$

$$\partial\theta/\partial\xi = \bar{u} = 0 \quad \text{on} \quad \xi = 0, l/d, \tag{15}$$

$$\partial\theta/\partial\eta = \bar{v} = 0 \quad \text{on} \quad \eta = 0, b/d. \tag{16}$$

where $\hat{\boldsymbol{\zeta}}$ is the unit vector in the $\zeta$ direction and the Rayleigh number $R$ is defined as

$$R = \alpha g\rho^2 K c d\Delta T/\mu k. \tag{17}$$

By taking the curl of Darcy's law, it can be seen that the vertical component of the vorticity is zero, i.e.

$$\partial\bar{v}/\partial\xi - \partial\bar{u}/\partial\eta = 0. \tag{18}$$

This is identically satisfied if

$$\bar{u} = \phi_{\zeta\xi}, \quad \bar{v} = \phi_{\zeta\eta}, \tag{19}$$

where the subscripts indicate differentiation. Furthermore, with

$$\bar{w} = -\phi_{\xi\xi} - \phi_{\eta\eta}, \tag{20}$$

we also satisfy the continuity equation. With the help of (19) and (20), we can obtain two equations for the unknowns $\theta$ and $\phi$ from (12) and (13):

$$\bar{\nabla}^2\phi = -R\theta, \tag{21}$$

$$\partial\theta/\partial\tau + \theta_\xi\phi_{\xi\zeta} + \theta_\eta\phi_{\eta\zeta} - (\phi_{\xi\xi}+\phi_{\eta\eta})\,\theta_\zeta = \bar{\nabla}^2\theta - \phi_{\xi\xi} - \phi_{\eta\eta}. \tag{22}$$

The boundary conditions on $\theta$ and $\phi$ are

$$\theta = \phi_{\xi\xi}+\phi_{\eta\eta} = \phi_{\zeta\zeta} = 0 \quad \text{on} \quad \zeta = 0, 1, \tag{23}$$

$$\theta_\xi = \phi_{\xi\zeta} = 0 \quad \text{on} \quad \xi = 0, l/d, \tag{24}$$

$$\theta_\eta = \phi_{\eta\zeta} = 0 \quad \text{on} \quad \eta = 0, b/d. \tag{25}$$

A single equation for $\phi$ can be derived from (21) and (22)

$$\partial\bar{\nabla}^2\phi/\partial\tau + \phi_{\xi\zeta}\bar{\nabla}^2\phi_\xi + \phi_{\eta\zeta}\bar{\nabla}^2\phi_\eta - (\phi_{\xi\xi}+\phi_{\eta\eta})\,\bar{\nabla}^2\phi_\zeta = \bar{\nabla}^4\phi + R(\phi_{\xi\xi}+\phi_{\eta\eta}). \tag{26}$$

The boundary conditions on $\phi$ are

$$\phi_{\xi\xi}+\phi_{\eta\eta} = \phi_{\zeta\zeta} = 0 \quad \text{on} \quad \zeta = 0, 1, \tag{27}$$

$$\phi_{\xi\zeta} = \bar{\nabla}^2\phi_\xi = 0 \quad \text{on} \quad \xi = 0, l/d, \tag{28}$$

$$\phi_{\eta\zeta} = \bar{\nabla}^2\phi_\eta = 0 \quad \text{on} \quad \eta = 0, b/d. \tag{29}$$

Following Straus (1974), who investigated two-dimensional convection in a layer of fluid-saturated porous material, we use the Galerkin technique to determine $\phi$ in this three-dimensional situation. The Fourier series expansion of $\phi$ is

$$\phi = \sum_{n=1}^{\infty}\sum_{j=0}^{\infty}\sum_{m=0}^{\infty}\phi_{njm}(\tau)\sin n\pi\zeta\cos\frac{j\pi\xi}{l/d}\cos\frac{m\pi\eta}{b/d}. \tag{30}$$

The boundary conditions (27)–(29) are identically satisfied by this form of the solution. Upon substituting (30) into (26) and using the orthogonality relations among the trigonometric functions, we obtain an infinite set of coupled, nonlinear, first-order ordinary differential equations for the $\phi_{njm}(\tau)$. These equations are solved numerically by truncating the infinite set; we retain only those terms which satisfy the requirement $n+j+m \leqslant N$, where $N$ is a positive integer.

To determine how large $N$ has to be for the solution of the truncated system to represent accurately convection in the box, we determine the dependence of the Nusselt number on $N$. The Nusselt number $Nu$, which is the dimensionless ratio of the horizontally averaged upward heat flux $q$ to that which would occur, in the absence of convection, by conduction alone, is given by

$$Nu \equiv \frac{q}{k\Delta T/d} = 1 - \sum_{n=1}^{\infty}\frac{n^3\pi^3}{R}\phi_{n00}(\tau=\infty). \tag{31}$$

We required that $N$ be sufficiently large that $Nu$ be accurate to within 1 %. Figure 1 shows how the calculated values of $Nu$ for three-dimensional convection depend on $N$. For $4{\cdot}5\pi^2 < R < 100$, $N = 8$ is adequate to satisfy this criterion, whereas for $100 < R < 150$, $N = 10$ is necessary. Many more terms are required to compute $Nu$ to a given accuracy for three-dimensional convection as compared with two-dimensional convection. Straus (1974) found that $N = 6$ was adequate to give $Nu$ accurate to 1 % for two-dimensional flows with $R$ as large as 150.

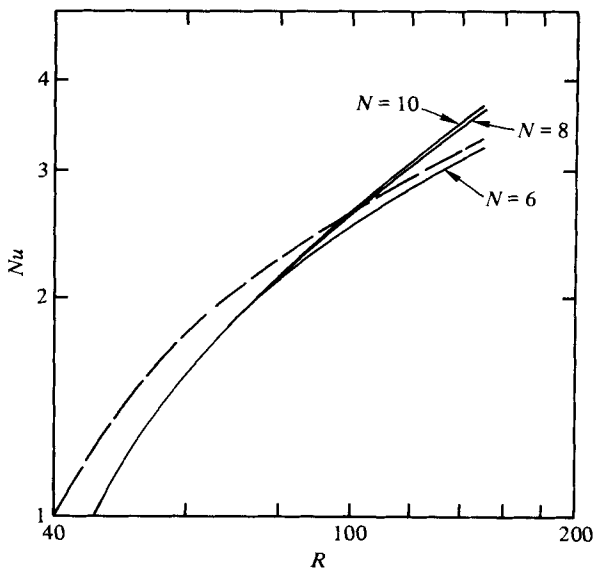


FIGURE 1. Nusselt number $Nu$ *vs.* Rayleigh number $R$ for two-dimensional (dashed curve) and three-dimensional (solid curves) convection in a cubic box of fluid-saturated porous material.

The complexity of the three-dimensional flows can be appreciated by noting that there are 56, 120 and 220 *a priori* non-zero coefficients with $N = 6$, 8 and 10 respectively, whereas the corresponding numbers of terms in two dimensions are 21, 36 and 55. In two dimensions, symmetry restricts the non-zero coefficients to those which have $n+j$ even (for unicellular flow), thus reducing the numbers of terms to 12, 20 and 30. In the next section, we shall see that steady-state three-dimensional convection in the range of Rayleigh numbers studied actually involves fewer non-zero coefficients than mentioned above.

## 3. Discussion of results

In order to investigate whether the 'dimensionality' of the convective flow in a cubic box of fluid-saturated porous material is completely determined by the Rayleigh number, or by the initial conditions, or by a combination of the two, the following numerical experiment was carried out. For a given value of $R$, the initial values of the coefficients $\phi_{njm}$ were chosen randomly in the range (0, 0·01). Two different sets of random initial values were used. In every case, a steady-state solution was reached, and both two- and three-dimensional solutions could be obtained at every value of $R$ in the range studied.

One of the sets of random initial values led to two-dimensional convection at Rayleigh numbers of 60, 70, 76, 82, 84, 90, 100 and 150 and three-dimensional convection at $R = 77$, 78, 80 and 81. The other set of initial values led to two-dimensional motion at $R = 60$ and 120 and three-dimensional flow at $R = 70$, 76, 80, 90, 100 and 110. Thus a given set of random initial conditions can give either two- or three-dimensional convection, depending on $R$. Accordingly, there appears to be no way to determine, from the characteristics of the random initial conditions alone, whether two- or

three-dimensional convection will result at a particular value of $R$. On the other hand, it is possible to force a specific type of convection by emphasizing a particular mode (e.g. $\phi_{111}$ or $\phi_{202}$) in the initial conditions.

One additional numerical experiment was carried out at $R = 120$. The initial values of one of the sets of modal coefficients were redistributed over the interval $(-0{\cdot}01, 0{\cdot}01)$ according to $\phi_{njm} \rightarrow 2\phi_{njm} - 0{\cdot}01$. Whereas the original set of initial conditions led to two-dimensional flow, the transformed set yielded three-dimensional motion.

In summary, then, at a given value of $R$, initial conditions determine whether the flow is two- or three-dimensional. There is no further non-uniqueness in the flow. At a given value of $R$, all two-dimensional flows were identical; the same can be said of the three-dimensional solutions.

Figure 1 shows the dependence of $Nu$ on $R$ for the two- and three-dimensional solutions. Two-dimensional convection transports more heat than does three-dimensional convection for Rayleigh numbers less than about 97; the reverse is true for $R \gtrsim 97$. Thus, even though two-dimensional flows have a higher Nusselt number at $R \lesssim 97$, three-dimensional convection is a possible steady state when the flows evolve from random initial conditions. Similarly, for $97 \lesssim R \lesssim 150$, two-dimensional convection is a possible final configuration for a system evolving from random initial states even though the two-dimensional states transport less heat. It would be interesting to determine if there is a value of $R$ above which the flow would evolve only to the three-dimensional configuration. Our previous calculations (Straus & Schubert 1978) suggest that two-dimensional convection in a cubic box would be stable at least up to $R = 400$.

Figures 2–4 illustrate different aspects of the three-dimensional convection patterns at $R = 80$ and 150. Figure 2 shows isotherms of the dimensionless temperature perturbation $\theta$ on the horizontal planes $\zeta = 0{\cdot}25$, $0{\cdot}50$ and $0{\cdot}75$. Figure 3 shows contours of constant horizontal velocity potential $\phi_\zeta$ on the horizontal planes $\zeta = 0$, $0{\cdot}25$, $0{\cdot}75$ and $1{\cdot}0$. Dimensionless velocity vectors on three faces of the box are shown in a perspective view in figure 4. All the figures include the fundamental three-dimensional mode $n = j = m = 1$ for comparison. Details regarding contour intervals, etc., are given in the figure captions.

Referring first to the $R = 80$ isotherms in figure 2, we see that the corners of the plane $\zeta = 0{\cdot}25$ are hot and cold centres. The hot (cold) spots are at diagonally opposite corners. The relatively hot fluid occupies a much smaller fraction of this plane than does the cold fluid. One can imagine narrow hot 'plumes' of rising fluid and much broader regions of descending cold fluid crossing this plane. By contrast, the isotherms of the $n = j = m = 1$ mode in this plane show no hot–cold asymmetry, while the hot corners at $R = 150$ occupy even smaller areas of the plane than they do at $R = 80$. In the midplane, $\zeta = 0{\cdot}5$, the isotherms of the $n = j = m = 1$ mode and of the flow at $R = 80$ and 150 are basically similar; hot and cold areas of the midplane are symmetric. The isotherms on the plane $\zeta = 0{\cdot}75$ are like those on the plane $\zeta = 0{\cdot}25$ with hot and cold regions reversed. The hot corners now occupy the greater area of the plane; i.e. hot plumes have broadened during their ascent. Nearly isothermal core regions elongated parallel to the diagonals of the horizontal planes $\zeta = 0{\cdot}25$ and $0{\cdot}75$ are apparent at $R = 80$ and 150; the isothermal cores are larger at $R = 150$ than at $R = 80$. Isotherms in the horizontal planes are symmetric about diagonals and display a sym-

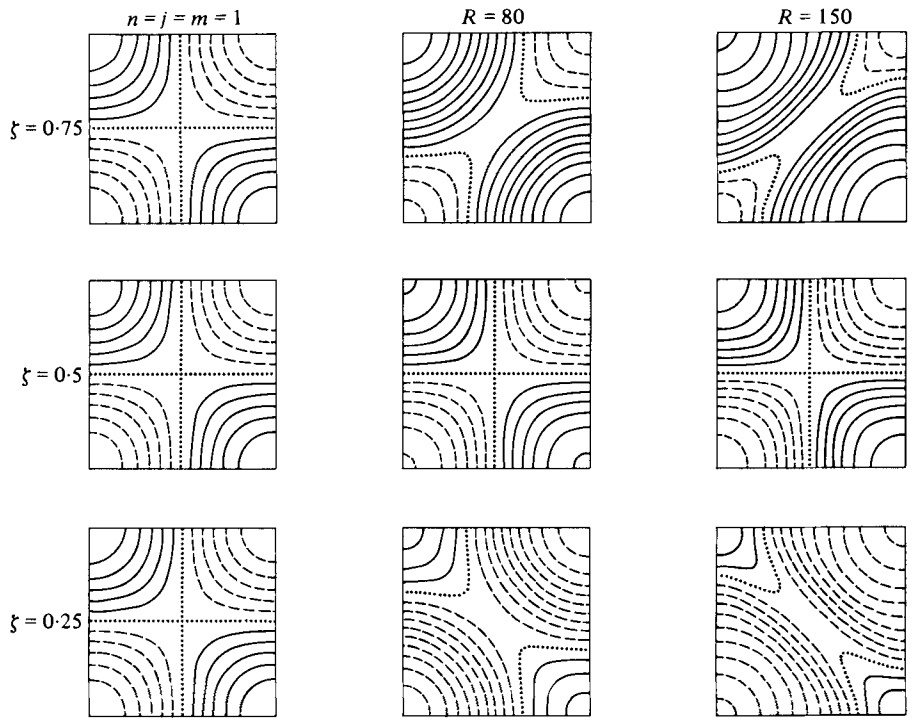


FIGURE 2. Isotherms of the dimensionless temperature perturbation $\theta$ on horizontal planes for three-dimensional convection at $R = 80$ and 150 and for a simple three-dimensional flow consisting of only the $n = j = m = 1$ term. At $R = 80$, the contour intervals are 0·05. At $R = 150$, the contour intervals on $\zeta = 0{\cdot}25$ and 0·75 are 0·06 but are 0·05 on the midplane $\zeta = 0{\cdot}5$. Hot isotherms are shown solid, cold ones are dashed. The $\theta = 0$ contours are dotted. For the $n = j = m = 1$ mode only the shapes of the isotherms are significant, i.e. the contour interval is arbitrary.

metry relative to the midplane. The cold fluid not only occupies a much larger area of the plane $\zeta = 0{\cdot}25$ than does the hot fluid, but the extremes of temperature are larger in the cold regions of the plane $\zeta = 0{\cdot}25$. A similar observation can be made for the hot areas of the plane $\zeta = 0{\cdot}75$.

The horizontal velocity potential $\phi_\xi$ contours shown in figure 3 describe the flow in horizontal planes. Since the horizontal velocity is the gradient of $\phi_\xi$, the horizontal velocities are orthogonal to the contours in the figure. The sense of the flow is from low to high values of $\phi_\xi$. The horizontal flow in the bottom plane, $\zeta = 0$, is outward from the cold corners and inward into the hot corners. In the top plane, $\zeta = 1{\cdot}0$, the horizontal flow is reversed; it is outward from the hot corners and inward into the cold corners. This can also be seen in the perspective views of the velocity vectors in the plane $\zeta = 1{\cdot}0$ in figure 4. The horizontal velocities in the horizontal planes are symmetric with respect to the diagonals and also exhibit a symmetry with respect to the midplane. The variations in contour spacing indicate where the horizontal motions are relatively fast and slow. This can also be seen by the lengths of the velocity vectors in the top plane of figure 4, although one must be careful to account for the foreshortening in this perspective view. In the bottom plane of figure 3, one can see that the areal extent of the outflow from the cold corners is equal to that of the inflow to the hot corners for the $n = j = m = 1$ mode. The inflow or outflow associated with each corner

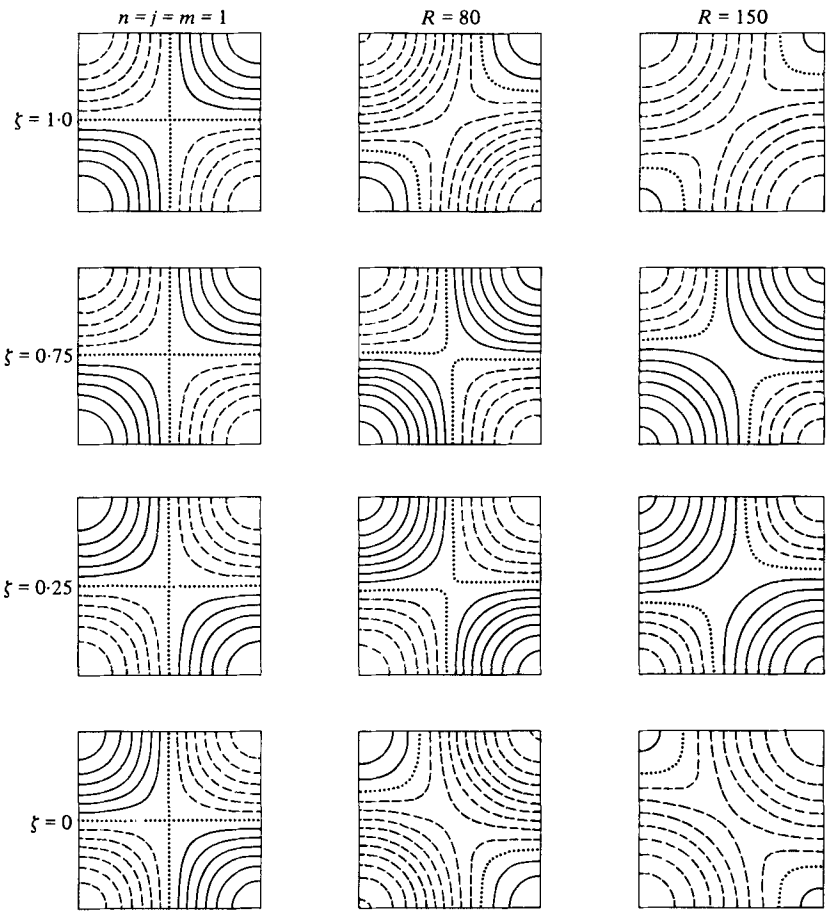


FIGURE 3. Contours of constant horizontal velocity potential $\phi_\zeta$ on the horizontal planes $\zeta = 0$, 0·25, 0·75, 1·0 for $R = 80$ and 150 and for the $n = j = m = 1$ mode. For $R = 80$, the contour interval is 0·3 on the planes $\zeta = 0{\cdot}25$ and 0·75 and 0·6 on the planes $\zeta = 0$ and 1. For $R = 150$, the contour interval is 0·6 on the planes $\zeta = 0{\cdot}25$, 0·75 and 2·0 on the planes $\zeta = 0$ and 1. Positive $\phi_\zeta$ contours are shown solid and negative contours are dashed. The $\phi_\zeta = 0$ contours are dotted. For the $n = j = m = 1$ mode, the contour intervals are arbitrary.

occupies a quarter of the area of the horizontal plane. At the high Rayleigh numbers however, the areal extent of the outflow from the cold corners exceeds that of the inflow to the hot corners, an effect which is more pronounced at $R = 150$ than at $R = 80$. This agrees qualitatively with what we deduced about the areal extent of hot and cold regions from the isotherm plot of figure 2. From figures 3 and 4, it can be seen that the diagonally elongated isothermal areas of the horizontal planes are associated with relatively low horizontal velocities.

The perspective view of the dimensionless velocity vectors on the three faces of the cubic box shown in figure 4 gives the most direct picture of the convection. The horizontal flow in the top plane can be seen moving outwards from above the hot upwelling plumes and inwards into the cold descending flow. The reduction in horizontal velocity along the diagonal connecting the cold corners in this plane as $R$ is increased is apparent. As can be seen by the flow in the vertical faces of figure 4,

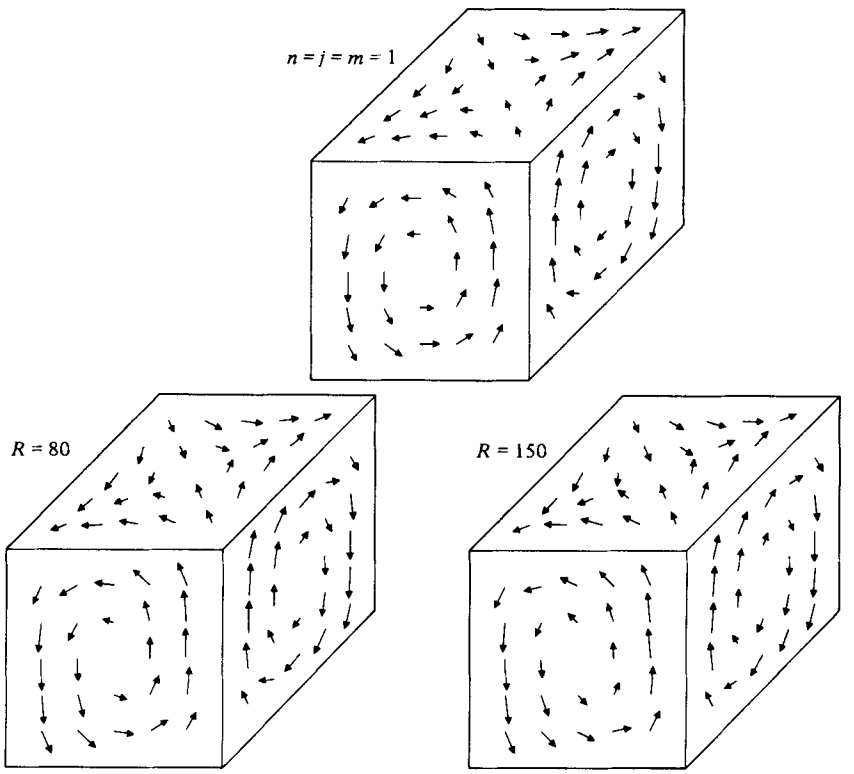


FIGURE 4. A perspective view of the dimensionless velocity vectors on three faces of the cubic box at $R = 80$ and 150 and for the $n = j = m = 1$ mode. The vector gives the velocity at the location of its tail. The length of each vector is proportional to the velocity, and the vectors are foreshortened according to the perspective. In the front face, the longest vector corresponds to a dimensionless velocity of 17 for $R = 80$ and 35 for $R = 150$.

upwelling and downwelling are symmetric for the $\phi_{111}$ mode. However, at $R = 80$ and 150, the ascending flow is wider above the midplane, while the descending flow is wider below the midplane.

Table 1 gives the largest coefficients $\phi_{njm}$ for the steady three-dimensional flows which we obtained at $R = 80$, 120 and 150 with $N = 10$. Convection at these Rayleigh numbers is dominated by the fundamental three-dimensional mode $n = j = m = 1$. The nonlinear interaction of this mode with itself produces the next largest (in absolute value) mode $\phi_{200}$ and the other significant modes $\phi_{222}$, $\phi_{202}$ and $\phi_{220}$. The third most important mode $\phi_{311}$ results from the nonlinear interactions of $\phi_{111}$ with all of the $n = 2$ modes.

Many of the coefficients not listed in table 1 are identically zero; in addition, several of the non-zero coefficients are equal. These properties can be understood in the following way. The steady-state equations and boundary conditions are invariant to an interchange of $\xi$ and $\eta$, leading to $\phi_{njm} = \phi_{nmj}$. (In a rectangular, rather than cubic, box this invariance would no longer exist.) We have seen in the previous discussion that $\theta$ (or $\phi$) is symmetric about diagonals of horizontal planes; this requires that $j+m$ be even. We have also seen that $\theta$ (or $\phi$) is antisymmetric with respect to a reflexion about the midplane $\zeta = \frac{1}{2}$ and a rotation of 90° about the line $\xi = \eta = \frac{1}{2}$; this requires that $n+m$ and $n+j$ be even also. These symmetries reduce the number of

| | $R = 80$ | $R = 120$ | $R = 150$ |
|---|---|---|---|
| $\phi_{200}$ | $-2{\cdot}618 \times 10^{-1}$ | $-5{\cdot}788 \times 10^{-1}$ | $-8{\cdot}209 \times 10^{-1}$ |
| $\phi_{400}$ | $-1{\cdot}080 \times 10^{-2}$ | $-3{\cdot}768 \times 10^{-2}$ | $-6{\cdot}345 \times 10^{-2}$ |
| $\phi_{600}$ | $-7{\cdot}556 \times 10^{-4}$ | $-4{\cdot}019 \times 10^{-3}$ | $-7{\cdot}774 \times 10^{-3}$ |
| $\phi_{800}$ | $-6{\cdot}791 \times 10^{-5}$ | $-5{\cdot}662 \times 10^{-4}$ | $-1{\cdot}314 \times 10^{-3}$ |
| $\phi_{202} = \phi_{220}$ | $-3{\cdot}077 \times 10^{-2}$ | $-5{\cdot}513 \times 10^{-2}$ | $-7{\cdot}385 \times 10^{-2}$ |
| $\phi_{402} = \phi_{420}$ | $-3{\cdot}291 \times 10^{-3}$ | $-6{\cdot}368 \times 10^{-3}$ | $-6{\cdot}825 \times 10^{-3}$ |
| $\phi_{602} = \phi_{620}$ | $-3{\cdot}529 \times 10^{-4}$ | $-1{\cdot}206 \times 10^{-3}$ | $-1{\cdot}984 \times 10^{-3}$ |
| $\phi_{204} = \phi_{240}$ | $-1{\cdot}813 \times 10^{-4}$ | $-1{\cdot}441 \times 10^{-3}$ | $-2{\cdot}186 \times 10^{-3}$ |
| $\phi_{111}$ | $1{\cdot}105 \times 10^{0}$ | $1{\cdot}798 \times 10^{0}$ | $2{\cdot}228 \times 10^{0}$ |
| $\phi_{311}$ | $6{\cdot}214 \times 10^{-2}$ | $1{\cdot}395 \times 10^{-1}$ | $1{\cdot}887 \times 10^{-1}$ |
| $\phi_{511}$ | $4{\cdot}983 \times 10^{-3}$ | $1{\cdot}705 \times 10^{-2}$ | $2{\cdot}696 \times 10^{-2}$ |
| $\phi_{711}$ | $4{\cdot}443 \times 10^{-4}$ | $2{\cdot}246 \times 10^{-3}$ | $4{\cdot}059 \times 10^{-3}$ |
| $\phi_{113} = \phi_{131}$ | $-7{\cdot}043 \times 10^{-3}$ | $-1{\cdot}241 \times 10^{-2}$ | $-1{\cdot}375 \times 10^{-2}$ |
| $\phi_{313} = \phi_{331}$ | $-2{\cdot}496 \times 10^{-3}$ | $-8{\cdot}844 \times 10^{-3}$ | $-1{\cdot}213 \times 10^{-2}$ |
| $\phi_{513} = \phi_{531}$ | $-1{\cdot}175 \times 10^{-4}$ | $-1{\cdot}140 \times 10^{-3}$ | $-1{\cdot}927 \times 10^{-3}$ |
| $\phi_{115} = \phi_{151}$ | $-4{\cdot}295 \times 10^{-5}$ | $-5{\cdot}796 \times 10^{-4}$ | $-1.138 \times 10^{-3}$ |
| $\phi_{222}$ | $2{\cdot}193 \times 10^{-2}$ | $7{\cdot}705 \times 10^{-2}$ | $1{\cdot}236 \times 10^{-1}$ |
| $\phi_{422}$ | $9{\cdot}643 \times 10^{-4}$ | $7{\cdot}941 \times 10^{-3}$ | $1{\cdot}446 \times 10^{-2}$ |
| $\phi_{622}$ | $-3{\cdot}517 \times 10^{-5}$ | $9{\cdot}465 \times 10^{-4}$ | $2{\cdot}641 \times 10^{-3}$ |
| $\phi_{224} = \phi_{242}$ | $-5{\cdot}778 \times 10^{-4}$ | $-3{\cdot}346 \times 10^{-3}$ | $-6{\cdot}134 \times 10^{-3}$ |
| $\phi_{424} = \phi_{442}$ | $-5{\cdot}075 \times 10^{-5}$ | $-1{\cdot}150 \times 10^{-3}$ | $-2{\cdot}782 \times 10^{-3}$ |
| $\phi_{133}$ | $2{\cdot}156 \times 10^{-3}$ | $8{\cdot}844 \times 10^{-3}$ | $2{\cdot}628 \times 10^{-2}$ |
| $\phi_{333}$ | $4{\cdot}538 \times 10^{-4}$ | $4{\cdot}840 \times 10^{-3}$ | $1{\cdot}032 \times 10^{-2}$ |
| $\phi_{244}$ | $1{\cdot}088 \times 10^{-4}$ | $1{\cdot}689 \times 10^{-3}$ | $4{\cdot}531 \times 10^{-3}$ |

TABLE 1. Values of $\phi_{njm}$ such that $|\phi_{njm}| > 10^{-3}$ for $R = 150$, $N = 10$.

non-zero coefficients from 220 to 55 (for $N = 10$) under steady-state conditions. There is no guarantee that these symmetries hold at arbitrarily large Rayleigh numbers.

## 4. Concluding remarks

We have found that three-dimensional convection in a cubic box of porous material is an easily realizable state at relatively low Rayleigh numbers, even down to the critical value. The same may not be true for rectangular boxes, since the unequal horizontal dimensions may introduce a preferred orientation for two-dimensional flow.

We have also observed that low Rayleigh number convection can be either two- or three-dimensional despite the fact that the three-dimensional flow transports less heat at $R \lesssim 97$. Thus the system does not act to maximize the heat transport, at least at low Rayleigh numbers. Rather, the final steady state at a given $R$ is determined by initial conditions. This importance of initial conditions may reflect the fact that the two- and three-dimensional Nusselt numbers differ by at most 12 % for $R \lesssim 150$. Perhaps at much higher Rayleigh numbers, where the three-dimensional heat transport greatly exceeds the two-dimensional one, three-dimensional convection will be preferred independent of initial conditions.

In view of the indeterminacy of the final steady-state configuration, it would be of interest to carry out a sufficient number of numerical experiments to determine whether it would be possible to characterize, from a probabilistic point of view, sets of random initial conditions which lead to a particular dimensionality of convection. Such an

investigation is beyond the scope of the present paper, but may constitute the subject of future research.

The authors wish to acknowledge useful discussions with G. M. Homsy and R. N. Horne. D. R. Hickman generated the perspective views of the flow field. This work was supported by the National Science Foundation under grant number ENG–76–82119.

## REFERENCES

BECK, J. L. 1972 Convection in a box of porous material saturated with fluid. *Phys. Fluids* **15**, 1377.

HOLST, P. H. & AZIZ, K. 1972 Transient three-dimensional natural convection in confined porous media. *Int. J. Heat Mass Transfer* **15**, 73.

HORNE, R. N. 1978 Three-dimensional natural convection in a confined porous medium heated from below. *A.I.A.A./A.S.M.E. Thermophys. Heat Transfer Conf.*

MALKUS, W. V. R. 1954 The heat transport and spectrum of thermal turbulence. *Proc. Roy. Soc.* A **225**, 196.

PLATZMAN, G. W. 1965 The spectral dynamics of laminar convection. *J. Fluid Mech.* **23**, 481.

STRAUS, J. M. 1974 Large amplitude convection in porous media. *J. Fluid Mech.* **64**, 51.

STRAUS, J. M. & SCHUBERT, G. 1978 On the existence of three-dimensional convection in a rectangular box of fluid-saturated porous material. *J. Fluid Mech.* **87**, 385.

ZEBIB, A. & KASSOY, D. R. 1978 Three-dimensional natural convection motion in a confined porous medium. *Phys. Fluids* **21**, 1.